

Theoretical Analysis of Multi-coding with Non-orthogonal Signaling

Brian Nelson and Behrouz Farhang-Boroujeny, *Life Senior Member, IEEE*

Abstract—Even though orthogonal multi-code signaling and its derivative, simplex signaling, are well known and widely used in different communication systems, certain applications may choose to adopt non-orthogonal signaling to benefit from other advantages that such signaling methods can offer. Motivated by a class of multi-carrier spread spectrum systems, this paper presents a thorough symbol error rate analysis of the broad class of multi-code signaling methods when they make use of codes which are not necessarily orthogonal. Our analysis is also extended to the case where the code set includes the negative of each code vector, i.e., an extension to biorthogonal signaling. Moreover, it is shown that the symbol error rate results derived in this paper reduce to those available in the literature when the multi-codes are orthogonal or satisfy the correlation property of simplex multi-codes.

I. INTRODUCTION

Orthogonal signaling is a well known communication technique, [1], [2]. It is widely used to increase the data rate of spread spectrum communication systems through a technique known as multi-coding. A multi-coded system makes use of an M -ary symbol alphabet to send information and is closely related to code division multiple access (CDMA) techniques. In CDMA, users are assigned unique codes that allow them to operate simultaneously over a shared channel. In multi-coding, multiple codes are assigned to a single user and can thus be used to increase the data rate of that user. This technique has been well studied and is often referred to as multi-code CDMA [3], [4].

Prior multi-coding works have used orthogonal signals to define the multi-codes, [3], [5], [6]. When the codes are chosen from a set of orthogonal signals, the symbol error probabilities are well-known and documented in textbooks, e.g., [1]. It also has been noted that one may add the negated versions of the orthogonal signals/codes into the set to double the size of the multi-code set, hence, one additional bit is added to each code symbol. The result is often referred to as biorthogonal signaling and is found to be optimal when the number of signal vectors is twice the dimensionality of the signal space [7]. Though orthogonal/biorthogonal signaling allows for simple probability of error analysis and may offer optimal performance in some cases, non-orthogonal signal sets may offer other performance advantages that warrant their use in certain applications.

The constant envelop orthogonal frequency division multiplexing phase modulation, known as OFDM-PM is a non-orthogonal signaling method that has been found to be of great value in certain applications because of its very low peak-to-average power ratio (PAPR), e.g., see [8]. The IEEE 802.15.4

wireless standard suggests a non-orthogonal frequency shift keying (FSK) method to improve on the bandwidth efficiency of transmission, [9]. Similarly, the authors of [10] use non-orthogonal FSK to reduce the bandwidth in a power line communication system. In [11], non-orthogonal signaling is used to reduce the complexity of an optical communication system.

Although non-orthogonal signaling has been found useful in a number of applications, theoretical study of the symbol error probabilities of such systems has remained very limited. Results have been derived only for some specific cases. For example, [12] has derived numerically tractable integrals for symbol error probability of multi-coding systems when the cross-correlation of all the codes are equal. These results are applied to find the probability of error for simplex signaling [13]. In simplex signaling, an orthogonal set of code vectors is replaced by a new set that is obtained by subtracting the mean of the first set from the respective code vectors. The new set is a non-orthogonal set, but as discussed in [13] offers a performance superiority over its orthogonal signaling counterpart; it requires a lower value of E_b/N_o (energy per bit over noise power spectral density) for a desired bit-error-rate (BER). This result is also well documented and can be found textbooks, e.g., [1]. Alternative derivations showing how the results for orthogonal signaling can be applied to simplex signaling are given in [1], [14]. For more general cases, others have concentrated on development of lower and upper bounds of symbol error probabilities, [8], [15], [16]. Many of these bounds are based on the work in [12] and in some cases have been acknowledged to be loose [17].

This paper has been motivated by our study of filter bank multi-carrier spread spectrum (FBMC-SS) where the symbol chips span over a set of subbands of the transmit signal, e.g., see [18], [19]. We have noted that, similar to the previous works, e.g., [1]–[4], to improve on the spectral efficiency of FBMC-SS, a multi-code signaling should be adopted. However, to be able to improve certain aspects of the system, we have found that non-orthogonal codes may prove useful. Unlike simplex signaling where correlations among code vectors remain the same for all the codes, here, correlations among code vectors may vary. One observation that we had in our study was that non-orthogonality of the code vectors, as long as they remain not far from an orthogonal case, have a negligible impact on the BER results. This small loss in BER performance motivated us to perform a deeper study of the non-orthogonal codes, develop theoretical results confirming our experimental findings, and possibly provide more insight. This general study covering the broad class of non-orthogonal

multi-codes and their biorthogonal counterparts, to the best of our knowledge, has never been presented in the past literature. Hence, the theoretical analysis presented in this paper may be found useful in other applications as well.

Although the developed theory in this paper is applicable to the broad class of multi-codes with any arbitrary code set, we have chosen to use the names “quasi-orthogonal” and “quasi-biorthogonal”. This misnomer of the terminologies is convenient and at the same time reflective of the cases of interest in practice.

FBMC-SS is known to be a superior waveform for rejection of partial-band interference, when compared to the more conventional method of direct sequence spread spectrum (DS-SS). This is because, in FBMC-SS, the spreading chips fall in different subcarrier bands and interference rejection is made possible by simply removing the interfered chips in the detection process. This process, obviously, is at the cost of a reduced processing gain. Moreover, when multi-codes are used, this process also leads to some loss of orthogonality of the residual spreading gain vectors. The theoretical method developed in this paper can be used to quantify the loss of performance caused by this loss of orthogonality.

A more recent work [20] has proposed FBMC-SS for ultra wide-band (UWB) communications. Additional study [21], [22] has revealed that filter banks based on offset quadrature amplitude modulation (FB-OQAM), also known as staggered multi-tone (SMT), [23], are the best choice in this application. It allows maximizing the transmit power while satisfying the spectral mask imposed by regulatory bodies; such as the Federal Communications Commission (FCC) in the United States. Moreover, to improve on the resiliency of the waveform to partial-band interferers, one may have to resort to using quasi-orthogonal codes. The use of quasi-orthogonal codes also allows reducing the PAPR of the transmit signal which is always desirable.

The rest of this paper is organized as follows. Section II is devoted to the case of quasi-orthogonal signaling. We show that the probability of a symbol error of such signaling methods can be formulated as an average of a set of multiple integrals. We show that this general result reduces to those reported in the literature for the case of orthogonal signaling by simply plugging in the respective correlation coefficients. For the case of simplex signaling, we show a simple modification to our derivations lead to the final results presented in equation (35) of [12]. Section III is devoted to the case of quasi-biorthogonal signaling. Here, we find that the derivation presented earlier for the quasi-orthogonal case can be easily extended to the case of quasi-biorthogonal signaling. In Section IV, we make use of a Monte Carlo integration technique to evaluate the multiple integrals developed in Sections II and III, with an affordable computational complexity. Section V is devoted to derivation of upper bounds for symbol error probabilities of both quasi-orthogonal and quasi-biorthogonal signaling methods. The numerical results presented in Section VI reveal that these bounds are very tight at the symbol error rates of practical interest ($< 10^{-3}$). The concluding remarks of the paper are made in Section VII.

Notations: Matrices, vectors, and scalar quantities are denoted by boldface uppercase, boldface lowercase, and normal letters, respectively. The element in the i th row and the j th column of a matrix \mathbf{R} is denoted as r_{ij} , and \mathbf{r}_j denotes the j th column of the same matrix. $\mathbb{E}[\cdot]$ denotes expectation, and \mathbf{I} refers to the identity matrix. The superscripts \cdot^T , \cdot^H , and \cdot^* indicate transpose, conjugate transpose, and conjugate operations, respectively. The Euclidean norm of a vector \mathbf{v} is denoted by $\|\mathbf{v}\|$. The notation $\mathcal{N}(\boldsymbol{\mu}, \boldsymbol{\Sigma})$ represents the normal distribution of a random vector with mean $\boldsymbol{\mu}$ and covariance matrix $\boldsymbol{\Sigma}$.

II. QUASI-ORTHOGONAL SIGNALING

A. System Model

We consider a communication system where the transmit information symbols are chosen from a set of real-valued length L alphabet vectors $\{\mathbf{s}_0, \mathbf{s}_1, \dots, \mathbf{s}_{M-1}\}$ which may not be orthogonal, but are linearly independent. Moreover, for $i = 0, \dots, M-1$, $\|\mathbf{s}_i\| = 1$. In addition, all symbol vectors are equally likely to be transmitted.

We consider an additive white Gaussian noise (AWGN) channel, where, when \mathbf{s}_i has been transmitted, the received signal vector is given as

$$\mathbf{x} = \sqrt{\mathcal{E}} \mathbf{s}_i + \mathbf{n}, \quad (1)$$

where \mathcal{E} is the received symbol energy, and \mathbf{n} is a channel noise vector with distribution $\mathbf{n} \sim \mathcal{N}(\mathbf{0}, \frac{N_0}{2} \mathbf{I})$.

To detect the transmitted information, we make use of the maximum likelihood (ML) decision rule, [1], where the receiver chooses

$$\hat{\mathbf{s}} = \arg \max_{\mathbf{s}_i} \mathbf{s}_i^T \mathbf{x}. \quad (2)$$

B. Symbol Error Probability Analysis

For the M -ary signaling discussed above, the probability of a symbol error may be given as

$$P_e = 1 - \frac{1}{M} \sum_{i=0}^{M-1} P_{c|\mathbf{s}_i} \quad (3)$$

where $P_{c|\mathbf{s}_i}$ refers to the probability of correct detection when the symbol vector \mathbf{s}_i has been transmitted. We note that because of different correlations among different symbol vectors, $P_{c|\mathbf{s}_i}$ should be calculated separately for all choices of $0 \leq i \leq M-1$.

Next, we note that

$$P_{c|\mathbf{s}_i} = \int \cdots \int_{D_i} f_X(\mathbf{x}) d\mathbf{x}, \quad (4)$$

where D_i indicates the decision region that corresponds to the ML decision rule (2), and $f_X(\mathbf{x})$ is the probability density function (PDF) of \mathbf{x} .

Note that in (4), the integral has the same dimension as the size of the signal vector \mathbf{x} , i.e., it is an M -fold integral. Computation of such integrals, even numerically, in general, may not be a straightforward task. In the sequel, we show how the integrals in (4) may be rearranged to allow numerical evaluation of $P_{c|\mathbf{s}_i}$, for all practical choices of M , that may be as large as a few hundreds.

We order the variables of integration so that the limits of the outer integrals do not depend on the variables of integration for the inner integrals. To this end, for a given choice \mathbf{s}_i , we organize the signal vectors $\{\mathbf{s}_0, \mathbf{s}_1, \dots, \mathbf{s}_{M-1}\}$ into a matrix

$$\mathbf{S}_i = [\mathbf{s}_i \quad \mathbf{s}_{i+1} \quad \dots \quad \mathbf{s}_{M-1} \quad \mathbf{s}_0 \quad \mathbf{s}_1 \quad \dots \quad \mathbf{s}_{i-1}] \quad (5)$$

of dimension $L \times M$. Let $\mathbf{S}_i = \mathbf{Q}\mathbf{R}$ be the QR factorization of \mathbf{S}_i , where \mathbf{Q} is an $L \times M$ matrix whose columns are an orthonormal basis set and \mathbf{R} is an $M \times M$ upper triangular matrix.

Before deriving the integration bounds, we make a few observations about \mathbf{Q} and \mathbf{R} . First, we note that the QR factorization is not unique and can always be chosen so that all diagonal elements of \mathbf{R} are non-negative. Moreover, for this choice of the QR factorization, one may choose to set $r_{00} = 1$. In that case, the first column of \mathbf{Q} will be equal to \mathbf{s}_i . Also, one may note that the orthonormality of the columns of \mathbf{Q} implies that the columns of \mathbf{R} are a set of unit length vectors, i.e., $\|\mathbf{r}_i\| = 1$, for $0 \leq i \leq M-1$.

Next, making use of (1), we define the length M vector

$$\begin{aligned} \mathbf{y} &= \mathbf{Q}^T \mathbf{x} \\ &= \sqrt{\mathcal{E}} \mathbf{r}_0 + \mathbf{n}' \end{aligned} \quad (6)$$

where $\mathbf{n}' = \mathbf{Q}^T \mathbf{n}$. Recalling that the columns of \mathbf{Q} are a set of orthonormal vectors, one finds that

$$\mathbf{y} \sim \mathcal{N}\left(\sqrt{\mathcal{E}} \mathbf{r}_0, \frac{N_0}{2} \mathbf{I}\right). \quad (7)$$

Moreover, (4) may be rewritten as

$$P_{c|\mathbf{s}_i} = \int \dots \int_{D'_i} f_Y(\mathbf{y}) d\mathbf{y} \quad (8)$$

where D'_i is the decision region for correct detection of \mathbf{r}_0 , and $f_Y(\mathbf{y})$ is the PDF of \mathbf{y} , given in (7).

Recalling (5), for any $j \neq i$, \mathbf{s}_j is transformed to

$$\mathbf{r}_{j'} = \mathbf{Q}^T \mathbf{s}_j \quad (9)$$

where

$$j' = \begin{cases} j - i, & j > i \\ M - i + j, & j < i. \end{cases} \quad (10)$$

Taking note that the vectors \mathbf{r}_0 and $\mathbf{r}_{j'}$ have unit length, the decision boundary between \mathbf{r}_0 and $\mathbf{r}_{j'}$ will be the hyperplane, [14],

$$(\mathbf{r}_0 - \mathbf{r}_{j'})^T \mathbf{y} = 0. \quad (11)$$

Hence, a correct decision is made when

$$(\mathbf{r}_0 - \mathbf{r}_{j'})^T \mathbf{y} > 0. \quad (12)$$

Next, taking note that \mathbf{R} is upper triangular and $r_{00} = 1$, (12) can be written as $y_0 - \sum_{i=0}^{j'} r_{k,j'} y_i > 0$, or, equivalently,

$$y_{j'} < u_{j'}(y_0, y_1, \dots, y_{j'-1}) \quad (13)$$

where

$$u_{j'}(y_0, y_1, \dots, y_{j'-1}) := \frac{y_0 - \sum_{k=0}^{j'-1} r_{k,j'} y_k}{r_{j',j'}}. \quad (14)$$

This is the upper limit of the $(j' + 1)^{th}$ inner integral in (8). Using these bounds, (8) can be written

$$P_{c|\mathbf{s}_i} = \int_{-\infty}^{\infty} \int_{-\infty}^{u_1(y_0)} \dots \int_{-\infty}^{u_{M-1}(y_0, y_1, \dots, y_{M-2})} f_Y(\mathbf{y}) d\mathbf{y}. \quad (15)$$

To convert (15) to a simpler form, we recall the distribution (7) and accordingly introduce the following change of variables

$$v_0 = \frac{y_0 - \sqrt{\mathcal{E}}}{\sqrt{\frac{N_0}{2}}} \quad (16)$$

and

$$v_i = \frac{y_i}{\sqrt{\frac{N_0}{2}}}, \quad \text{for } i = 1, 2, \dots, M-1, \quad (17)$$

to rearrange (15) as in (18) at the top of the next page. In (18), $f(x)$ is the standard normal function defined as

$$f(x) = \frac{1}{\sqrt{2\pi}} e^{-\frac{1}{2}x^2}. \quad (20)$$

C. Extensions to the Known (Trivial) Cases

In the current literature one will find equations for the symbol error rates of multi-codes for a couple of specific cases. Here, we show how the above results of the general case may be simplified to reduce to those in the literature.

1) *Orthogonal Case*: When the code set $\{\mathbf{s}_0, \mathbf{s}_1, \dots, \mathbf{s}_{M-1}\}$ consists of a set orthogonal vector, QR decomposition \mathbf{S} has the trivial solution $\mathbf{S}\mathbf{I}$. That is, \mathbf{R} is the identity matrix \mathbf{I} , hence, $r_{j,j} = 1$ and for $j < k$, $r_{j,k} = 0$. For this particular case, (19) reduces to

$$u'_j(v_0, v_1, \dots, v_{j-1}) = v_0 + \sqrt{\frac{2\mathcal{E}}{N_0}}, \quad (21)$$

whose application in (18) leads to the well known result [1, pg. 205]

$$P_{c|\mathbf{s}_i} = \int_{-\infty}^{\infty} f(v_0) \left(\int_{-\infty}^{v_0 + \sqrt{\frac{2\mathcal{E}}{N_0}}} f(v_1) dv_1 \right)^{M-1} dv_0. \quad (22)$$

2) *Equi-Correlated Case*: The equi-correlated case that was first studied in [12] considers the case where

$$\mathbf{S}^T \mathbf{S} = \mathbf{W} = \begin{bmatrix} 1 & \eta & \dots & \eta \\ \eta & 1 & \dots & \eta \\ \vdots & \vdots & \ddots & \eta \\ \eta & \eta & \dots & 1 \end{bmatrix}. \quad (23)$$

We take note that the matrix \mathbf{S} is of size $L \times M$ and its columns are the alphabet vectors $\mathbf{s}_0, \mathbf{s}_1, \dots$, and \mathbf{s}_{M-1} . Accordingly, η is the correlation between any pair of these alphabet vectors and \mathbf{W} is a positive semi-definite matrix of size $M \times M$. In simplex signaling $\eta = -\frac{1}{M-1}$ and $L = M$.

Consider the eigen-decomposition

$$\mathbf{W} = \mathbf{V} \mathbf{\Lambda} \mathbf{V}^T, \quad (24)$$

where the columns of \mathbf{V} are the eigenvectors of \mathbf{W} and $\mathbf{\Lambda}$ is a diagonal matrix with eigenvalues of \mathbf{W} at its diagonal. Taking note that

$$\mathbf{W} = \eta \mathbf{1}\mathbf{1}^T + (1 - \eta) \mathbf{I}, \quad (25)$$

$$P_{c|s_i} = \int_{-\infty}^{\infty} f(v_0) \int_{-\infty}^{u'_1(v_0)} f(v_1) \cdots \int_{-\infty}^{u'_{M-1}(v_0, v_1, \dots, v_{M-2})} f(v_{M-1}) dv_{M-1} \cdots dv_1 dv_0, \quad (18)$$

where

$$u'_j(v_0, v_1, \dots, v_{j-1}) = \frac{1}{r_{j,j}} \left[(1 - r_{0,j}) \left(v_0 + \sqrt{\frac{2\mathcal{E}}{N_0}} \right) - \sum_{k=1}^{j-1} r_{k,j} v_k \right] \quad (19)$$

it is straightforward to show that the eigenvalues of \mathbf{W} are $\lambda_0 = 1 + (M-1)\eta$, and for $1 \leq i \leq M-1$, $\lambda_i = 1 - \eta$. We also take note that $\mathbf{\Lambda}$ can be written as

$$\mathbf{\Lambda} = \eta M \mathbf{B} + (1 - \eta) \mathbf{I}, \quad (26)$$

where $\mathbf{B} = \text{diag}([1, 0, \dots, 0])$.

Next, we recall that a square root of \mathbf{W} can be found as

$$\mathbf{U} = \mathbf{V} \mathbf{\Lambda}^{\frac{1}{2}} \mathbf{V}^T. \quad (27)$$

Like the matrix $\mathbf{\Lambda}$, the matrix $\mathbf{\Lambda}^{\frac{1}{2}}$ can be also split into two matrices as

$$\mathbf{\Lambda}^{\frac{1}{2}} = a \mathbf{B} + b \mathbf{I} \quad (28)$$

where

$$a = \sqrt{(M-1)\eta + 1} - \sqrt{1 - \eta} \quad (29)$$

and

$$b = \sqrt{1 - \eta}. \quad (30)$$

Making use of this observation, one finds that

$$\mathbf{U} = \begin{bmatrix} d & c & \cdots & c \\ c & d & \cdots & c \\ \vdots & \vdots & \ddots & c \\ c & c & \cdots & d \end{bmatrix}, \quad (31)$$

where

$$c = \frac{1}{M} \left(\sqrt{1 + \eta(M-1)} - \sqrt{1 - \eta} \right) \quad (32)$$

and

$$d = \sqrt{1 - \eta} + c. \quad (33)$$

Considering the above results, one may conclude that the matrix \mathbf{S} that carries the symbol alphabets as its columns has the general form

$$\mathbf{S} = \mathbf{Q} \mathbf{U} \quad (34)$$

where \mathbf{Q} is a matrix of size $L \times M$ with a set of unit length orthogonal vectors as its columns. Here, given the simple and special form of the matrix \mathbf{U} ,

We also take note that given the symmetry of the matrix \mathbf{U} , the symbol error probabilities are independent of the choice of the transmitted symbol. Hence, without any loss of generality, we consider the case where \mathbf{s}_0 has been transmitted. Thus, using (1), with \mathbf{s}_i replaced by \mathbf{s}_0 , one finds that

$$\begin{aligned} \mathbf{y} &= \mathbf{Q}^T \mathbf{x} \\ &= \sqrt{\mathcal{E}} \mathbf{u}_0 + \mathbf{n}' \end{aligned} \quad (35)$$

where $\mathbf{n}' = \mathbf{Q}^T \mathbf{n}$.

Here, the decision boundary for making a correct decision is found to be

$$(\mathbf{u}_0 - \mathbf{u}_i)^T \mathbf{y} > 0. \quad (36)$$

Substituting the relevant columns of \mathbf{U} in (36), and taking note that $d - c = \sqrt{1 - \eta}$ is a positive number, (36) reduces to

$$y_i < y_0, \quad (37)$$

for $1 \leq i \leq M-1$. This leads to the following equation for the probability of a correct decision

$$P_c = \int_{-\infty}^{\infty} f_{Y_0}(y_0) \left(\int_{-\infty}^{y_0} f_{Y_1}(y_1) dy_1 \right)^{M-1} dy_0. \quad (38)$$

Recognizing that

$$\mathbf{y} \sim \mathcal{N} \left(\sqrt{\mathcal{E}} \mathbf{u}_0, \frac{N_0}{2} \mathbf{I} \right) \quad (39)$$

and applying the conversions to standard normal following (16) and (17) in (38), we get

$$P_c = \int_{-\infty}^{\infty} f(v_0) \left(\int_{-\infty}^{v_0 + \sqrt{\frac{2\mathcal{E}(1-\eta)}{N_0}}} f(v_1) dv_1 \right)^{M-1} dv_0. \quad (40)$$

This result is similar to that of the orthogonal case with the received signal energy scaled by a factor equal to $1 - \eta$. This result is in perfect agreement with the probability of correct symbol detection reported in [12]; see equation (35) and the following paragraph in this paper.

III. QUASI-BIORTHOGONAL SIGNALING

A. System Model

Here, we extend the above results to the case where the alphabet vectors are extended to the following set

$$\begin{aligned} \mathbf{s}_0 &= -\mathbf{s}_M \\ \mathbf{s}_1 &= -\mathbf{s}_{M+1} \\ &\vdots \\ \mathbf{s}_{M-1} &= -\mathbf{s}_{2M-1}. \end{aligned} \quad (41)$$

As before, the vectors $\mathbf{s}_0, \mathbf{s}_1, \dots, \mathbf{s}_{M-1}$ may not be orthogonal, but are linearly independent. We also assume that the detector uses the maximum likelihood (ML) decision rule, [1], where the receiver first computes

$$z_i = \mathbf{s}_i^T \mathbf{x} \text{ for } 0 \leq i < M, \quad (42)$$

and subsequently obtains the estimate of the transmitted symbol as

$$\hat{\mathbf{s}} = \text{sign}(z_k) \mathbf{s}_k, \text{ where } k = \arg \max_{0 \leq i < M} |z_i|. \quad (43)$$

B. Symbol Error Probability Analysis

The probability of a decision error can be found using (3), but due to the symmetry of the signal set, the probability of error is the same for both \mathbf{s}_i and $-\mathbf{s}_i$. Hence, (3) is applicable to the case here as well. Moreover, as in the case of orthogonal signaling, here also $P_{c|\mathbf{s}_i}$ can be found by finding the decision region and integrating the PDF over that region. The decision boundaries are obtained by following the same line of derivations as in Section II-B. The difference here is that in addition to the upper bounds in the integrals, there are also a set of lower bounds. While the upper bounds are those obtained using (12), the lower bounds are obtained using the inequality

$$(\mathbf{r}_0 + \mathbf{r}_{j'})^T \mathbf{y} > 0. \quad (44)$$

Following the same line of derivations to those in Section II-B, one will find that (44) leads to

$$y_{j'} > l_{j'}(y_0, y_1, \dots, y_{j'-1}), \quad (45)$$

where

$$l_{j'}(y_0, y_1, \dots, y_{j'-1}) := \frac{-y_0 - \sum_{k=0}^{j'-1} r_{k,j'} y_k}{r_{j',j'}}. \quad (46)$$

In addition, here, the detector should distinguish between \mathbf{r}_0 and $-\mathbf{r}_0$. The decision boundary between \mathbf{r}_0 and $-\mathbf{r}_0$ is the hyperplane orthogonal to \mathbf{r}_0 and passing through the origin. This can be written as

$$y_0 > 0. \quad (47)$$

This specifies the limits of integration in the outer integral.

Considering the above points, one will find that

$$P_{c|\mathbf{s}_i} = \int_0^\infty \int_{l_1(y_0)}^{u_1(y_0)} \dots \int_{l_{M-1}(y_0, y_1, \dots, y_{M-2})}^{u_{M-1}(y_0, y_1, \dots, y_{M-2})} f_Y(\mathbf{y}) d\mathbf{y}. \quad (48)$$

Making use of (16) and (17), this result can be rewritten in terms of the standard normal PDFs. The result is presented in (49) at the top of the next page.

For the case where the symbol vectors \mathbf{s}_0 through \mathbf{s}_{M-1} are an orthogonal set, \mathbf{R} will be an identity matrix (see the discussion in Section II-C1) and as a result (49) reduces to

$$P'_{c|\mathbf{s}_i} = \int_{-\sqrt{\frac{2\epsilon}{N_0}}}^\infty f(v_0) \left(\int_{-v_0 - \sqrt{\frac{2\epsilon}{N_0}}}^{v_0 + \sqrt{\frac{2\epsilon}{N_0}}} f(v_1) dv_1 \right)^{M-1} dv_0. \quad (51)$$

This is in perfect agreement with those reported in the literature; e.g., see [1, pg. 208].

IV. NUMERICAL CALCULATION P_e

To determine P_e , we must evaluate the integral given in (18), in the case of quasi-orthogonal signaling, or (49), in the case of quasi-biorthogonal signaling and apply (3). The dimensionality of the integrals is M , with no apparent method for simplification. To evaluate the integrals, we turn to Monte Carlo integration techniques. This approach has been applied across a wide variety of disciplines and has proven effective in efficiently evaluating high dimensional integrals [24]. Here, we

show how the integral in (18) or (49) can be formulated and solved to a desired precision using Monte Carlo integration techniques.

To evaluate an integral using Monte Carlo techniques, one may formulate the integral as computing the expected value of a function $g(X)$ of a random variable (R.V.), and then design an estimator of that function. If the estimator is consistent, its value will approach the expected value as the number of samples increases.

In our case, we define the functions

$$g_i(\mathbf{v}) = \begin{cases} 1 & \mathbf{v} \in D_i \\ 0 & \text{otherwise,} \end{cases} \quad \text{for } 0 \leq i \leq M-1 \quad (52)$$

where D_i , as defined before, refers to the domain of the multidimensional integral in (18) or (49). Accordingly, the desired estimator for each $P_{c|\mathbf{s}_i}$ is formulated as

$$\begin{aligned} P_{c|\mathbf{s}_i} &= \int_{-\infty}^\infty \dots \int_{-\infty}^\infty g_i(\mathbf{v}) f_{\mathbf{V}}(\mathbf{v}) d\mathbf{v} \\ &\approx \frac{1}{K} \sum_{k=0}^{K-1} g_i(\mathbf{V}_k) \\ &:= G_i, \end{aligned} \quad (53)$$

where $f_{\mathbf{V}}(\mathbf{v})$ is the multivariate Gaussian PDF $\mathcal{N}(\mathbf{0}, \frac{N_0}{2}\mathbf{I})$ and G_i indicates the estimator result for $P_{c|\mathbf{s}_i}$. Because the desired result is P_e , we form an estimator of P_e as

$$G = \frac{1}{M} \sum_{i=0}^{M-1} G_i. \quad (54)$$

To find G , we evaluate $g_i(\mathbf{V})$ by drawing K independent and identically distributed (IID) samples from $f_{\mathbf{V}}(\mathbf{v})$, denoted by \mathbf{v}_k , and insert the results in (53). The function $g_i(\mathbf{v})$ is evaluated following (52), by checking if \mathbf{v} is within the bounds defined by D_i . This process is repeated for each \mathbf{s}_i and the estimate of P_e is computed using (54). Hence, the total number of samples of \mathbf{v} used to obtain an estimate of G is KM .

To find the number of samples K required per estimator G_i that achieves a certain accuracy in the estimate G , we make use of the Chebychev inequality, [24, pg. 23]. For the case here, the Chebychev inequality states that

$$\Pr \left\{ |G - \mathbb{E}[G]| \geq \left[\frac{\text{var}[G]}{\delta} \right]^{\frac{1}{2}} \right\} \leq \delta, \quad (55)$$

where δ is a (small) constant and $\text{var}[\cdot]$ denotes variance of. To proceed, we first note that (53) and (54) imply

$$\begin{aligned} \text{var}[G] &= \frac{1}{KM^2} \sum_{i=0}^{M-1} \text{var}[g_i(\mathbf{V})] \\ &= \frac{1}{KM} \text{avg}_i (\text{var}[g_i(\mathbf{V})]). \end{aligned} \quad (56)$$

Moreover, since $g_i(\mathbf{V})$ is a binary random variable, it has a Bernoulli distribution with parameter $p = P_{c|\mathbf{s}_i} = 1 - P_{e|\mathbf{s}_i}$, hence, $\text{var}[g_i(\mathbf{V})] = P_{e|\mathbf{s}_i}(1 - P_{e|\mathbf{s}_i})$.

$$P_{c|s_i} = \int_{-\sqrt{\frac{2\mathcal{E}}{N_0}}}^{\infty} f(v_0) \int_{u'_1(v_0)}^{u'_1(v_0)} f(v_1) \cdots \int_{u'_{M-1}(v_0, v_1, \dots, v_{M-2})}^{u'_{M-1}(v_0, v_1, \dots, v_{M-2})} f(v_{M-1}) dv_{M-1} \cdots dv_1 dv_0, \quad (49)$$

where $u'_j(v_0, v_1, \dots, v_{j-1})$ is given in (19) and

$$u'_j(v_0, v_1, \dots, v_{j-1}) = \frac{1}{r_{j,j}} \left[-(1 + r_{0,j}) \left(v_0 + \sqrt{\frac{2\mathcal{E}}{N_0}} \right) - \sum_{k=1}^{j-1} r_{k,j} v_k \right]. \quad (50)$$

Taking note that our interest is mostly centered around the points where the probability $P_{e|s_i}$ is small, say $P_{e|s_i} < 0.01$, one may argue $P_{e|s_i}(1 - P_{e|s_i}) \approx P_{e|s_i}$ and, hence,

$$\text{avg}_i(\text{var}[g_i(\mathbf{V})]) \approx P_e. \quad (57)$$

Another point that should be taken note of is the fact that $\mathbb{E}[G] = 1 - P_e$ and $G = 1 - \hat{P}_e$, where \hat{P}_e is an estimate of P_e . These imply

$$|G - \mathbb{E}[G]| = |P_e - \hat{P}_e| \quad (58)$$

Making use of (56), (57) and (58), (55) may be rearranged as

$$\Pr \left\{ |P_e - \hat{P}_e| \geq \left[\frac{P_e}{KM\delta} \right]^{\frac{1}{2}} \right\} \leq \delta. \quad (59)$$

Considering (59), one may argue for \hat{P}_e to be close estimate of P_e (equivalently, G be a good approximation to $P_c = \mathbb{E}[G]$), one may let

$$\left[\frac{P_e}{KM\delta} \right]^{\frac{1}{2}} = \epsilon P_e, \quad (60)$$

where ϵ is a small constant. Solving (60) for KM , i.e., the number of samples required to obtain a good estimate of P_e , we get

$$KM = \frac{1}{\delta \epsilon^2 P_e}. \quad (61)$$

In (61), we are facing a problem where KM , on the left-hand side, depends on the quantity P_e , on the right-hand side, which we are seeking to estimate. This dilemma may be solved by replacing P_e by the known probability of symbol error, p_e , from an equivalent orthogonal multi-code. That is, KM is obtained using

$$KM = \frac{1}{\delta \epsilon^2 p_e}, \quad (62)$$

instead of (61). Since, $p_e < P_e$, (62) may be thought as an over-estimate of KM .

The interesting result here is that KM is independent of the number of integrals in (18) or (49). To get a feel of how large KM should be, we note that the choices of $\delta = \epsilon = 0.01$ are reasonable, and with these choices, (62) reduces to

$$KM = \frac{10^6}{p_e}. \quad (63)$$

Then, when $p_e = 0.01$, $KM = 10^8$, and this value increases by an order of magnitude for each decrement of p_e by an order of magnitude. This allows measuring P_e values as low as 10^{-6} in a reasonable amount of time, even for the cases where M grows to a few hundreds. It is also worth noting

that for small values of p_e (in the range of 10^{-5} or smaller), the upper bound developed in the next section is very tight, thus, provides an accurate estimate of the desired probability of symbol error.

V. DEVELOPMENT OF AN UPPER BOUND

Although the probability of a symbol error can be found using the methods discussed in Sections II and III and numerically evaluated as discussed in Section IV, it may be still desirable if one could avoid evaluation of the Monte Carlo integrals. In this section, we derive an upper bound that becomes exceedingly tight over the SNR range of practical interest. This derivation builds on an alternative derivation (different from those developed in Section II and Section III) of the exact probability of error for the quasi-biorthogonal signaling when $M = 2$. The alternative derivation presented for this special case is also instructive in visualizing the robustness (a minimum performance loss) of quasi-orthogonal/biorthogonal signaling methods when compared to their orthogonal/biorthogonal counterparts.

A. Quasi-Biorthogonal Signaling for the Case $M = 2$

For this special case, the set of signaling alphabets are the vectors $\{\pm \mathbf{s}_0, \pm \mathbf{s}_1\}$ of length $L \geq 2$. Without any loss of generality, consider the case where $+\mathbf{s}_0$ has been transmitted. Then, the received signal is

$$\mathbf{x} = \sqrt{\mathcal{E}} \mathbf{s}_0 + \mathbf{n}. \quad (64)$$

In the presentation that follows, we concentrate on the signal vectors within the plane spanned by the vectors \mathbf{s}_0 and \mathbf{s}_1 . We note that, for $L > 2$, the noise vector \mathbf{n} may have components both in the plane spanned by the vectors \mathbf{s}_0 and \mathbf{s}_1 and perpendicular to it. We also take note that the latter component of \mathbf{n} has no impact on the symbol decision in the case of interest here and, thus, may be removed from the right-hand side of (64). Considering this, we assume \mathbf{n} in (64) refers to the component of the noise within the plane spanned by the vectors \mathbf{s}_0 and \mathbf{s}_1 .

The decision boundaries around \mathbf{s}_0 are in the direction of the lines $\mathbf{d}_0^T \mathbf{x} = 0$ and $\mathbf{d}_1^T \mathbf{x} = 0$ where

$$\mathbf{d}_0 = \frac{\mathbf{s}_0 - \mathbf{s}_1}{\|\mathbf{s}_0 - \mathbf{s}_1\|} \quad (65)$$

and

$$\mathbf{d}_1 = \frac{\mathbf{s}_0 + \mathbf{s}_1}{\|\mathbf{s}_0 + \mathbf{s}_1\|}. \quad (66)$$

These decision boundaries and a choice of the received signal vector \mathbf{x} are presented in Fig. 1(a) along with the shaded

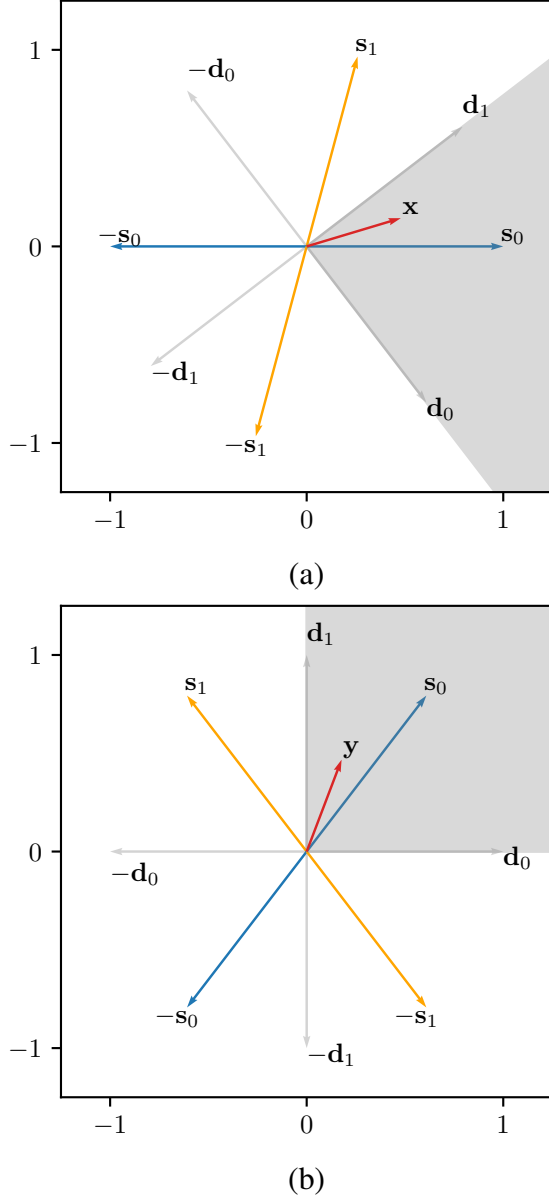


Fig. 1. The signal vectors, decision boundaries, and an example of the received signal vector when the signal set is $\{\pm s_0, \pm s_1\}$. In (a), these vectors are shown in the original space, and (b) shows the vectors in the coordinate system of \mathbf{d}_0 and \mathbf{d}_1 . In both cases the decision region for $+s_0$ is shaded.

decision region to correctly select $+s_0$. Here, we see that although s_0 and s_1 are not orthogonal, the decision boundaries are orthogonal and span the same space as the one spanned by s_0 and s_1 . The orthogonality of \mathbf{d}_0 and \mathbf{d}_1 can be verified by observing that $\mathbf{d}_0^T \mathbf{d}_1 = 0$.

To evaluate the probability of a symbol error, we start by defining the matrix

$$\mathbf{D} = [\mathbf{d}_0 \quad \mathbf{d}_1], \quad (67)$$

and use the columns of this matrix as an orthogonal basis set to evaluate the probability of a symbol error. This is done by finding \mathbf{x} in the coordinates defined by the basis set \mathbf{d}_0 and

\mathbf{d}_1 . This is obtained as

$$\begin{aligned} \mathbf{y} &= \mathbf{D}^T \mathbf{x} \\ &= \sqrt{\mathcal{E}} \mathbf{D}^T \mathbf{s}_0 + \mathbf{n}' \end{aligned} \quad (68)$$

where $\mathbf{y} \sim \mathcal{N}(\sqrt{\mathcal{E}} \mathbf{D}^T \mathbf{s}_0, \frac{N_0}{2} \mathbf{I})$. This operation can be seen in Fig. 1(b), where we see that the decision boundaries form the basis axes of the transformed signal space. Accordingly, the probability of a correct symbol decision can be calculated as

$$P_c = \int_0^\infty \int_0^\infty f(\mathbf{y}) d\mathbf{y}. \quad (69)$$

To evaluate this probability, we let

$$\mathbf{z} = \frac{\mathbf{y} - \sqrt{\mathcal{E}} \mathbf{D}^T \mathbf{s}_0}{\sqrt{\frac{N_0}{2}}} \quad (70)$$

and note that the elements z_0 and z_1 of \mathbf{z} are a pair of independent, zero-mean, and unit variance random variables. Making use of this result in (69), one will find that

$$P_c = \left(\int_{-\sqrt{\frac{2\mathcal{E}\rho_0^2}{N_0}}}^\infty f(z_0) dz_0 \right) \left(\int_{-\sqrt{\frac{2\mathcal{E}\rho_1^2}{N_0}}}^\infty f(z_1) dz_1 \right), \quad (71)$$

where $\rho_k = \mathbf{d}_k^T \mathbf{s}_0$ for $k = 0, 1$, and $f(\cdot)$, as defined earlier, is the standard normal function. Making use of the Q function, [25, pg. 21], (71) reduces to

$$P_c = \prod_{k=0}^1 \left[1 - Q \left(\sqrt{\frac{2\mathcal{E}\rho_k^2}{N_0}} \right) \right], \quad (72)$$

Hence, the probability of a symbol error is given by

$$\begin{aligned} P_e &= 1 - P_c \\ &= 1 - \prod_{k=0}^1 \left[1 - Q \left(\sqrt{\frac{2\mathcal{E}\rho_k^2}{N_0}} \right) \right]. \end{aligned} \quad (73)$$

At this point it is instructive to look at the symbol constellation points resulting from the code vectors \mathbf{s}_0 and \mathbf{s}_1 in the Cartesian plane introduced by the basis set \mathbf{d}_0 and \mathbf{d}_1 . This is visualized in Fig. 2, where the quasi-biorthogonal signal vectors are chosen with $\mathbf{s}_0^T \mathbf{s}_1 = 0.25$. When \mathbf{s}_0 and \mathbf{s}_1 are orthogonal, the constellation points resemble those of a quadrature phase shift keying (QPSK) modulation. Any non-orthogonality of \mathbf{s}_0 and \mathbf{s}_1 results in a rotation of QPSK points along the unit circle towards either the horizontal or the vertical axis.

The rotation of the QPSK points can be calculated by making use of the equation

$$\theta = \cos^{-1} \left(\frac{1}{\sqrt{2}} (\mathbf{d}_0 + \mathbf{d}_1)^T \mathbf{s}_0 \right). \quad (74)$$

This is the angle between the unit length vectors \mathbf{s}_0 and the bisect of basis vectors \mathbf{d}_0 and \mathbf{d}_1 . In the case presented in Fig. 2, where $\mathbf{s}_0^T \mathbf{s}_1 = 0.25$, one will find that $\theta = 7.2^\circ$. As one may see from Fig. 2, this translates to a small performance loss for such a relatively large loss of orthogonality. This is in line with the numerical results that are presented in the next section.

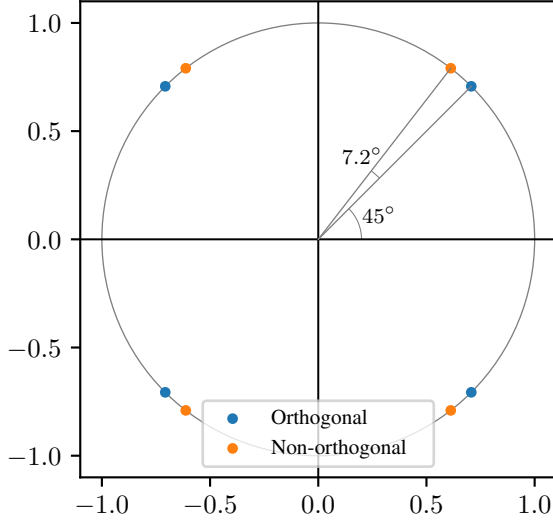


Fig. 2. Constellation in terms of the basis formed by the decision boundaries $[\mathbf{d}_0 \ \mathbf{d}_1]$ when the signal vectors are orthogonal and not orthogonal.

B. Upper Bound for Quasi-Biorthogonal Signaling

Here, we divert our attention to the case where $M > 2$. Let A_{i+} be the event of detecting $+\mathbf{s}_i$, and A_{i-} be the event of detecting $-\mathbf{s}_i$. Then, the probability of a symbol error given $+\mathbf{s}_i$ was transmitted is given by

$$P_{e|s_i} = \Pr \left[\bigcup_{\substack{j=0 \\ j \neq i}}^{M-1} (A_{j+} \cup A_{j-}) \cup A_{i-} \mid +\mathbf{s}_i \text{ sent} \right]. \quad (75)$$

The right-hand side of (75) should be stated as the probability of one or more the indicated events happens. Then, taking note that for any pair of events A and B , $\Pr[A \cup B] \leq \Pr[A] + \Pr[B]$, (75) implies

$$P_{e|s_i} \leq \sum_{\substack{j=0 \\ j \neq i}}^{M-1} \Pr[A_{j+} \cup A_{j-} \cup A_{i-} \mid +\mathbf{s}_i \text{ sent}]. \quad (76)$$

Making use of the results in Section V-A, this result can be written as

$$P_{e|s_i} \leq \sum_{\substack{j=0 \\ j \neq i}}^{M-1} \left(1 - \prod_{k=0}^1 \left[1 - Q \left(\sqrt{\frac{2\mathcal{E}\rho_{i,j,k}^2}{N_0}} \right) \right] \right) \quad (77)$$

where

$$\begin{aligned} \rho_{i,j,0} &= \frac{(\mathbf{s}_i - \mathbf{s}_j)^T \mathbf{s}_j}{|\mathbf{s}_i - \mathbf{s}_j|} \\ \rho_{i,j,1} &= \frac{(\mathbf{s}_i + \mathbf{s}_j)^T \mathbf{s}_j}{|\mathbf{s}_i + \mathbf{s}_j|}. \end{aligned} \quad (78)$$

Using (77) and assuming that the data symbols $\pm\mathbf{s}_i$, for $i = 0, 1, \dots, N-1$, are equally likely to be transmitted, one

will find that the probability of a symbol error, P_e , is upper bounded by

$$P_e \leq \frac{1}{M} \sum_{i=0}^{M-1} \sum_{\substack{j=0 \\ j \neq i}}^{M-1} \left(1 - \prod_{k=0}^1 \left[1 - Q \left(\sqrt{\frac{2\mathcal{E}\rho_{i,j,k}^2}{N_0}} \right) \right] \right). \quad (79)$$

The simulation results presented in the next section reveal that this upper bound becomes tight as the SNR increases. This observation may be explained as follows. As the SNR increases, the events referred to on the right-hand side of (75) become nearly non-overlapping, equivalently, it will be unlikely that any pair of these events happen simultaneously. In that case, the inequality in (76) will become closer to an equality.

C. Upper Bound for Quasi-Orthogonal Signaling

The desired bound here can be derived following those of the biorthogonal case with some minor modifications. First, for the case where $M = 2$, the decision boundary that separates \mathbf{s}_0 and \mathbf{s}_1 is the bisect line between them. This is the line in the direction \mathbf{d}_1 in Fig. 1(a). With this observation, the probability of a symbol error here is found to be

$$P_e = Q \left(\sqrt{\frac{2\mathcal{E}\rho_0^2}{N_0}} \right). \quad (80)$$

Next, following the same line of thoughts as those in Section V-B, and removing A_{j-} and A_{i-} from the right-hand side (75) and subsequent equations, it is not hard to arrive at the following upper bound for probability of symbol error for the present case.

$$P_e \leq \frac{1}{M} \sum_{i=0}^{M-1} \sum_{\substack{j=0 \\ j \neq i}}^{M-1} Q \left(\sqrt{\frac{2\mathcal{E}\rho_{i,j,0}^2}{N_0}} \right) \quad (81)$$

VI. NUMERICAL RESULTS

In this section, to get insight to the theoretical findings of the previous sections, we present a set of numerical results that compare the symbol error rates (SERs) of the quasi-orthogonal and quasi-biorthogonal signaling methods against their respective orthogonal and biorthogonal counterparts. The goal here is to explore the amount of performance loss incurred as the non-orthogonality of the symbol vectors increases. Also, through numerical results, we examine the tightness of the upper bounds that were derived in Section V.

Here, to generate a set of non-orthogonal codes, we begin with generating a random correlation matrix \mathbf{W} with diagonal elements of unity. For \mathbf{W} to be a valid correlation matrix, it should be symmetric, i.e., $\mathbf{W}^T = \mathbf{W}$, and all of its eigenvalues should be non-negative. To satisfy these conditions, first, the off diagonal elements in the upper triangular part of \mathbf{R} are chosen to be random and independent taken from a uniform distribution in the interval $[-\rho_{\max}, +\rho_{\max}]$. These elements are then copied to the lower triangular part of \mathbf{W} so that to satisfy the symmetry condition $\mathbf{W}^T = \mathbf{W}$. Finally, to make

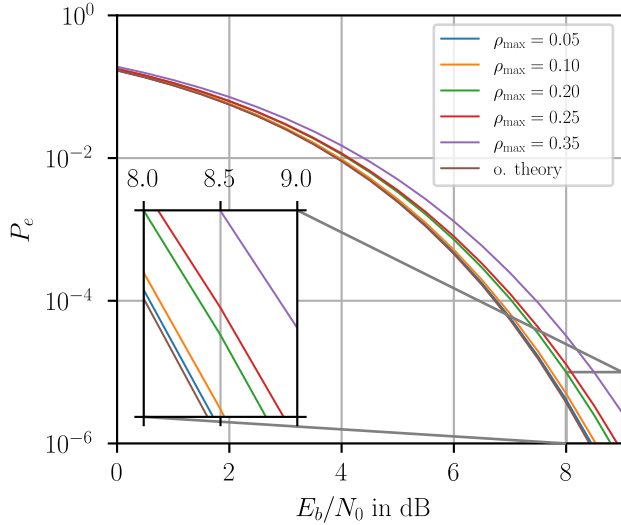


Fig. 3. SER, P_e , results for a range of non-orthogonal multi-codes. A lower bound given by the result arising from a set of orthogonal codes is included for reference.

sure that \mathbf{W} is a valid correlation matrix, its eigenvalues are examined to be all non-negative. In case the latter condition is not satisfied, another random choice of \mathbf{W} is generated until a proper choice \mathbf{W} is obtained.

Once we have found a proper correlation matrix \mathbf{W} , we find the matrix \mathbf{S} which satisfies the equality $\mathbf{S}^T \mathbf{S} = \mathbf{W}$, hence, columns of \mathbf{S} are the desired multi-code symbol vectors. A matrix \mathbf{S} that satisfies the equality $\mathbf{S}^T \mathbf{S} = \mathbf{W}$ is often referred to as a square-root of \mathbf{W} . The common method of finding the square-root of a non-negative definite matrix \mathbf{W} is to first perform the factorization $\mathbf{W} = \mathbf{V} \mathbf{\Lambda} \mathbf{V}^T$, where columns of \mathbf{V} are eigenvectors of \mathbf{W} and $\mathbf{\Lambda}$ is a diagonal matrix with the eigenvalues of \mathbf{W} at its diagonal elements, and then set $\mathbf{S} = \mathbf{V} \mathbf{\Lambda}^{\frac{1}{2}} \mathbf{V}^T$.

Fig. 3 presents the SER results of quasi-orthogonal coding for the case where $M = 16$. A few choices of the parameter ρ_{\max} are examined. The SER plots, here, are found using the Monte Carlo integration techniques developed in Section IV. The SER plot of the orthogonal coding is also presented as a bench-mark. As one would expect from our observations in Section V, for small choices of $\rho_{\max} < 0.1$, the non-orthogonality of multi-code vectors incurs very little loss in performance. The performance loss is about 0.4 dB when $\rho_{\max} = 0.2$, and is slightly above 1 dB when ρ_{\max} is set to a high value 0.35.

Similar results to those in Fig. 3 are obtained when the same code sets are applied to a quasi-biorthogonal signaling. The SER curves for the biorthogonal case will be shifted to the left by about 0.5 dB.

Fig. 4 shows the upper bound derived in Section V-C for the quasi-orthogonal signaling scheme with $M = 16$ and $\rho_{\max} = 0.2$. As can be seen, the upper bound becomes very tight at the symbol error rates of practical interest ($P_e < 10^{-3}$).

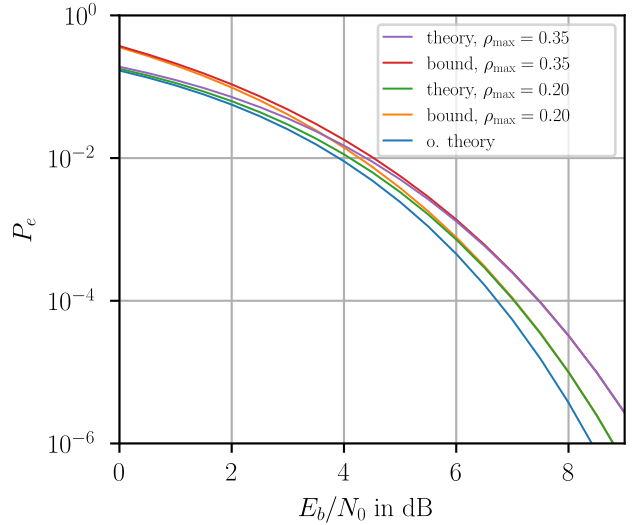


Fig. 4. SER, P_e , results for non-orthogonal multi-codes with $\rho_{\max} = 0.2$ and $\rho_{\max} = 0.35$. A lower bound arising from a set of orthogonal codes and upper bounds given by (81) are also presented.

VII. CONCLUSION

A set of compact equations for symbol error probabilities of a general class of multi-coding systems, where the correlation among different code vectors can be any arbitrary value, were derived. The derivation includes both quasi-orthogonal and quasi-biorthogonal signaling methods. The use of Monte Carlo integration was introduced for numerical calculation of the symbol error rates (SERs) of the studied cases. It was noted that this numerical method allows accurate evaluations of SERs down to the values as low as 10^{-6} with an affordable computational complexity. In addition, we developed equations for tight upper bounds of SERs of interest. These upper bounds provide accurate estimates of the SERs in the cases where their numerical calculation may be infeasible.

ACKNOWLEDGEMENTS

This research made use of Idaho National Laboratory's High Performance Computing systems located at the Collaborative Computing Center and supported by the Office of Nuclear Energy of the U.S. Department of Energy and the Nuclear Science User Facilities under Contract No. DE-AC07-05ID14517.

This manuscript has in part been authored by Battelle Energy Alliance, LLC under Contract No. DE-AC07-05ID14517 with the U.S. Department of Energy. The United States Government retains and the publisher, by accepting the paper for publication, acknowledges that the United States Government retains a nonexclusive, paid-up, irrevocable, worldwide license to publish or reproduce the published form of this manuscript, or allow others to do so, for United States Government purposes. STI Number: INL/JOU-24-77579.

REFERENCES

- [1] J. G. Proakis, *Digital Communications*, 5th ed. New York, NY, USA: McGraw-Hill, 2008.

- [2] M. K. Simon, *Digital Communication Techniques: Signal Design and Detection*. Englewood Cliffs, N.J., USA: Prentice Hall, 1994.
- [3] H. Liu, "Multicode ultra-wideband scheme using chirp waveforms," *IEEE Journal on Selected Areas in Communications*, vol. 24, no. 4, pp. 885–891, 2006.
- [4] J. Zhu, H. Zhang, and Y. Gu, "Principle and performance of variable rate multi-code CDMA method," in *Proceedings of ICUPC '95 - 4th IEEE International Conference on Universal Personal Communications*. IEEE, 1995, pp. 256–259.
- [5] D. B. Haab, H. Moradi, and B. Farhang-Boroujeny, "Filter bank multi-carrier spread spectrum with biorthogonal signaling for high speed data transmission through HF skywave channels," in *MILCOM 2018 - 2018 IEEE Military Communications Conference (MILCOM)*. IEEE, 2018, pp. 1–9.
- [6] T. Ohta and K. Ohuchi, "Method for extending parallel combinatory multi-code transmission with constant-amplitude signaling," in *The Sixth International Workshop on Signal Design and Its Applications in Communications*. IEEE, 2013, pp. 12–15.
- [7] C. Weber, "New solutions to the signal design problem for coherent channels," *IEEE transactions on information theory*, vol. 12, no. 2, pp. 161–167, 1966.
- [8] S. Thompson, A. Ahmed, J. Proakis, and J. Zeidler, "Constant envelope OFDM phase modulation: spectral containment, signal space properties and performance," in *IEEE MILCOM 2004. Military Communications Conference, 2004.*, vol. 2, 2004, pp. 1129–1135 Vol. 2.
- [9] "IEEE standard for low-rate wireless networks—amendment 2: Low power wide area network (LPWAN) extension to the low-energy critical infrastructure monitoring (LECI) physical layer (PHY)," *IEEE Std 802.15.4w-2020 (Amendment to IEEE Std 802.15.4-2020 as amended by IEEE Std 802.15.4z-2020)*, pp. 1–46, 2020.
- [10] A. K. Pandey, K. Reeshitha, and S. P. Dash, "Error analysis and optimization of m-ary frequency-shift-keying modulation for coherent PLC systems in nakagami-m environment," *IEEE transactions on vehicular technology*, vol. 71, no. 6, pp. 5896–5905, 2022.
- [11] Y. Q. Hong, "Non-orthogonal PS-OOK transmission for FSO communications," *Optics continuum*, vol. 1, no. 9, p. 1970, 2022.
- [12] A. Nuttall, "Error probabilities for equicorrelated m-ary signals under phase-coherent and phase-incoherent reception," *IRE Transactions on Information Theory*, vol. 8, no. 4, pp. 305–314, 1962.
- [13] A. D. Wyner, "On coding and information theory," *SIAM Review*, vol. 11, no. 3, pp. 317–346, 1969. [Online]. Available: <http://www.jstor.org/stable/2028940>
- [14] A. Balakrishnan, "A contribution to the sphere-packing problem of communication theory," *Journal of Mathematical Analysis and Applications*, vol. 3, no. 3, pp. 485–506, 1961. [Online]. Available: <https://www.sciencedirect.com/science/article/pii/0022247X61900725>
- [15] L. Rugini and G. Baruffa, "Performance of nonorthogonal FSK for the internet of things," *Digital Signal Processing*, vol. 85, pp. 124–133, 2019. [Online]. Available: <https://www.sciencedirect.com/science/article/pii/S1051200418305542>
- [16] W. Lindsey and M. Simon, "L-orthogonal signal transmission and detection," *IEEE Transactions on Communications*, vol. 20, no. 5, pp. 953–960, 1972.
- [17] I. Jacobs, "Comparison of m-ary modulation systems," *The Bell System Technical Journal*, vol. 46, no. 5, pp. 843–864, 1967.
- [18] D. L. Wasden, H. Moradi, and B. Farhang-Boroujeny, "Design and implementation of an underlay control channel for cognitive radios," *IEEE journal on selected areas in communications*, vol. 30, no. 10, pp. 1875–1889, 2012.
- [19] S. A. Laraway and B. Farhang-Boroujeny, "Performance analysis of a multicarrier spread spectrum system in doubly dispersive channels with emphasis on HF communications," *IEEE Open Journal of the Communications Society*, vol. 1, pp. 462–476, 2020.
- [20] B. Farhang-Boroujeny, H. Moradi, and T. V. Holschuh, "Filter bank UWB communications," *IEEE Communications Magazine*, pp. 120–125, January 2024.
- [21] B. Nelson, H. Moradi, and B. Farhang-Boroujeny, "Uwb narrowband interference survey and design considerations," 2024. [Online]. Available: <https://arxiv.org/abs/2411.07052>
- [22] —, "Filter-banks for ultra-wideband communications: Advantages and design challenges," 2024. [Online]. Available: <https://arxiv.org/abs/2411.05989>
- [23] B. Farhang-Boroujeny, "OFDM versus filter bank multicarrier," *IEEE signal processing magazine*, vol. 28, no. 3, pp. 92–112, 2011.
- [24] M. H. Kalos, *Monte Carlo Methods*, 2nd ed. Weinheim, Germany: Wiley-Blackwell, 2008.
- [25] S. M. Kay, *Fundamentals of Statistical Signal Processing: Detection Theory*. Englewood Cliffs, NJ, USA: Prentice-Hall, 1998.